Available online at www.sciencedirect.com
ScienceDirect
Journal of Hydrodynamics
2008,20(2):164-171
ELSEVIER
www.sciencedirect.com/
science/journal/10016058

INVESTIGATION OF AIRSHIP AEROELASTICITY USING FLUID-STRUCTURE INTERACTION*

LIU Jian-min, LU Chuan-jing, XUE Lei-ping
Department of Engineering Mechanics, Shanghai Jiaotong University, Shanghai 200240, China,
E-mail: liujm@sjtu.edu.cn

(Received March 19, 2007, Revised April 16, 2007)

Abstract: Due to the flexibility of the envelope of large stratosphere airships, the aerodynamic solution of such airship is closely related to its shape and the external aerodynamic forces which lead to the structural deformation. It is essentially one of the Fluid-Structure Interaction (FSI) problems. This article aims at the numerical investigation of nonlinear airship aeroelasticity in consideration of aerodynamics and structure coupling, using an iteration method. The three-dimensional flow around the airship was numerically studied by means of the SIMPLE method based on the finite volume method. Nonlinear finite element analysis was employed for geometrically nonlinear deformation of the airship shape. Comparison of aerodynamic parameters and the pressure distribution between rigid and aeroelastic models was conducted when an airship is in a trimmed flight state in specified flight conditions. The effect of aeroelasticity on the airship aerodynamics was detailed.

Key words: airship, three-dimensional flow, elastic deformation, fluid-structure interaction

1. Introduction

The design of stratosphere airships is different from other vehicles in two particular features:

(1) The airship requires large volume which provides enough buoyancy to keep it stay in the stratosphere, where the density of air is only as much as one thirteenth of that on the sea level.

(2) The light material is adopted in order to meet the demand for small weight of the airship, which results in the considerable flexibility of the whole envelope.

For such features, the flexible hull of the airship undergoes shape changes under external forces, meanwhile, the shape variations affect the pattern and structure of its surrounding fluid flow. This is a problem of static aeroelasticity. That is, load distribution occurs because the deformation of the airship influences the distribution of aerodynamic pressures over the structure. To get accurate results, the complete behavior of the airship in real flow conditions should be simulated, taking into account the hull deformation in different flowing situations. This is possible with coupled CFD and CSD simulation.

Coupled fluid-structure studies have been the subject of a large amount of development in the last two decades. Engineering applications of aeroelasticity studies are in their great majority concerned with aircraft domains. However, published aeroelastic studies about airships remain rare [1]. Wang and Shan [2] adopted a panel method to estimate the aerodynamic force of stratosphere airships. But the aeroelasticity effect had not been taken into account in their work. With the help of ABAQUS and the software VSAERO which is based on potential flow theory, Bessert and Frederich[1] investigated the influence of aerodynamics on the structural behaviour of the airship. In this paper a three-dimensional model is developed to account for the nonlinear deformation of the airship interacting with viscous flows. For a typical airship in steady flight, part of the aerodynamic drag owes its origin to the bare hull and the remaining is generated by fins, gondolas, and engines. The bare hull drag could account for about 60%-70% of the total, the proportion increasing with

* **Biography:** LIU Jian-min(1972-), Male, Ph. D. Student

the airship size as the appendages become smaller in relation to the hull [3]. At the first stage in our study, more attention was paid to the bare hull, the envelope of the airship, which is considered as a membrane structure. The Green-Lagrange strain tensor is employed for the description of large deformation. A nonlinear finite element method was introduced for solving the structure equations of the airship. The flow solver is derived based on the Reynolds-averaged Navier-Stokes equations. A Thin Plate Spline (TPS) is adopted as the interface to exchange the information between the fluid and structure computations.

2. Mathematic model of fluid flow around airship

In this section, the fluid flow solver and the physical model of fluid dynamics are presented. The governing equations of fluid flow are the mass conservation equation and Reynolds-averaged Navier-Stokes equations. For simulating turbulent we employ the standard k-ε two model (Jones and Launder 1972) and *LL*-Low Reynolds modified model[4-6] . The unknown functions, which will be solved later, are the velocity components $\underline{u} = (u, v, w)$ in the $x-$, $y-$ and $z-$ directions, pressure p , kinetic energy of turbulence k, and dissipation ε .

The mass conservation equation and the three-dimensional Navier-Stokes equations for incompressible flow can be written as

$$\frac{\partial \rho}{\partial t} + \frac{\partial \rho U_j}{\partial x_j} = 0 \tag{1}$$

$$\frac{\partial \rho U_j}{\partial t} + \frac{\partial U_i U_j}{\partial x_j} = -\frac{\partial P}{\partial x_j} + \frac{\partial}{\partial x_j} \bullet$$

$$\left[(\mu + \mu_T) \left(\frac{\partial U_i}{\partial x_j} + \frac{\partial U_j}{\partial x_i} \right) \right] \tag{2}$$

The kinetic energy equation is expressed as

$$\rho \frac{\partial k}{\partial t} + \rho U_j \frac{\partial k}{\partial x_j} = P - \rho\varepsilon + \frac{\partial}{\partial x_j} \bullet$$

$$\left[(\mu + \mu_T) \frac{\partial k}{\partial x_j} \right] \tag{3}$$

The dissipation equation is

$$\rho \frac{\partial \varepsilon}{\partial t} + \rho U_j \frac{\partial \varepsilon}{\partial x_j} = f_1 C_{\varepsilon 1} \frac{\varepsilon}{k} P - f_2 C_{\varepsilon 2} P \frac{\varepsilon^2}{k} +$$

$$\frac{\partial}{\partial x_j} \left[\left(\mu + \mu_T \frac{\mu_T}{Pr_z} \right) \frac{\partial \varepsilon}{\partial x_j} \right] \tag{4}$$

where

$$f_1 = 1 + \frac{P}{P^*}, \ f_2 = 1 - 0.3\mathrm{e}^{-R_t^2},$$

$$f_\mu = \frac{1 - \mathrm{e}^{-\alpha_\mu R_k}}{1 - \mathrm{e}^{-\alpha_\varepsilon R_k}}, \ R_t = \frac{k^2}{\nu\varepsilon},$$

$$R_k = \frac{\sqrt{k}n}{\nu}, \ P^* = \frac{f_2 C_{\varepsilon 2} k^{1.5}}{C_{\varepsilon 1} L_\varepsilon} \mathrm{e}^{-\alpha_d R_k^2},$$

$$L_\varepsilon = \kappa c_\mu^{0.75} n (1 - \mathrm{e}^{-\alpha_\varepsilon R_k}), \ C_{\varepsilon 1} = 1.44,$$

$$C_{\varepsilon 2} = 1.92, \ Pr_k = 1, \ Pr_\varepsilon = 1.3,$$

$$\alpha_d = 0.0022, \ \alpha_\varepsilon = 0.263, \ \alpha_\mu = 0.016$$

The coefficient of eddy viscosity μ_T is defined by

$$\mu_T = \rho f_\mu c_\mu \frac{k^2}{\varepsilon} \tag{5}$$

To solve the equations of fluid flow, proper boundary conditions are required. At the inlet boundary, the inflow velocity is given. At the outlet boundary, extrapolation of the velocity, kinetic energy of turbulence and dissipation to the boundary (zero gradient) can usually be used for steady flows when the outflow boundary is far from the region of interest. At the interface between fluid and airship surface, the non-slip condition is applied.

3. Numerical solver for fluid flow and airship structure

The basic method of fluid simulation is pressure correction method and the finite volume is used for numerical discretization[7, 8].

The computational code is programmed by the authors. The validity of the results from this program has been evaluated against different kinds of velocities from incompressible flow to transonic flow and

supersonic flow, in internal and external flow fields, respectively. The turbulent model mentioned above is sufficiently accurate for two-dimensional flows, and fairly accurate for complicated three-dimensional flows where there is no separating zone. However, it should be noted that although a great deal has been learnt for simple flows, there is not a comprehensive and complete turbulent model which can effectively describe the physical characters of turbulent flow when the flow has great separating zones. Nor can the k - ε two-equation model. Because of this, there may be some difference between computational results and real conditions.

The stratosphere airship is generally designed as nonrigid. The principal structural component, the envelope, is made of fabric membrane material with small Young's modulus, which is sensitive to load. Though the strain in the structure when under load is small, i.e., the fiber extension and angle changes between fibers are small, the deformation of the airship membrane structure can be comparatively large[9, 10]. Thus the influence of the inherent nonlinear structure must be taken into account. With this consideration, we obtain the following strain-displacement relation with nonlinear terms reflecting large deformation:

$$\varepsilon_X = \frac{\partial u}{\partial X} + \frac{1}{2}\left[\left(\frac{\partial u}{\partial X}\right)^2 + \left(\frac{\partial v}{\partial X}\right)^2 + \left(\frac{\partial w}{\partial X}\right)^2\right] \tag{6a}$$

$$\varepsilon_Y = \frac{\partial v}{\partial Y} + \frac{1}{2}\left[\left(\frac{\partial u}{\partial Y}\right)^2 + \left(\frac{\partial v}{\partial Y}\right)^2 + \left(\frac{\partial w}{\partial Y}\right)^2\right] \tag{6b}$$

$$\varepsilon_{XY} = \frac{1}{2}\left(\frac{\partial v}{\partial X} + \frac{\partial u}{\partial Y}\right) + \frac{1}{2}\left(\frac{\partial u}{\partial X}\frac{\partial u}{\partial Y} + \frac{\partial v}{\partial X}\frac{\partial v}{\partial Y} + \frac{\partial w}{\partial X}\frac{\partial w}{\partial Y}\right) \tag{6c}$$

where u, v, w are displacements in the X, Y, Z directions, respectively, from the unstrained position in initial coordination system.

In a linear analysis, it is assumed that the displacement is infinitesimally small so there is no difference between Cauchy stress and second Piola-Kirchoff stress. However, in an analysis of large deformation, the Cauchy stress referred to the deformed geometry is the real stress on the structure, while the second Piola-Kirchhoff stress is the expression of the Cauchy stress in current configuration with respect to the initial coordinate. This is an important difference compared with linear analysis. In the constitute relations, the second Piola-Kirchhoff stress tensor $\boldsymbol{S}$ is used frequently, which is work-conjugate with the Green tension tensor. That is,

$$\boldsymbol{S} = \boldsymbol{C}\boldsymbol{\varepsilon} \tag{7}$$

in which $\boldsymbol{C}$ is the material matrix of membrane. It should be recognized that the second Piola-Kirchhoff stress has little physical meaning and, in practice, the Cauchy stress must be calculated.

Consider elastic membrane, which in its initial state occupies a finite region in space. In global coordinate, the general form of the principle of virtual work in Lagrangian description is given by

$$\int_v \delta \boldsymbol{E}^T \sigma \mathrm{d}v = \int_v \delta \boldsymbol{u}^T q \mathrm{d}v + \int_A \delta \boldsymbol{u}^T p \mathrm{d}A \tag{8}$$

where $\delta \boldsymbol{u}^T$ are the virtual displacements, $\delta \boldsymbol{E}^T$ represent the corresponding virtual strains, p is the external surface force, and q is the body force.

In the present work of structure analysis, a spatial triangular membrane element is employed. The bending rigidity and transverse shear rigidity of membrane structure are negligible. Each node has three degrees of freedom and each membrane with three nodes has nine degrees of freedom. If the element is sufficiently small, the displacement at any point within the element can be approximated with a linear combination of displacement of nodes. That is, the shape function of membrane element is[11]

$$N = \frac{1}{2A}\bullet$$

$$\begin{bmatrix} N_1 & 0 & 0 & N_2 & 0 & 0 & N_3 & 0 & 0 \\ 0 & N_1 & 0 & 0 & N_2 & 0 & 0 & N_3 & 0 \\ 0 & 0 & N_1 & 0 & 0 & N_2 & 0 & 0 & N_3 \end{bmatrix} \tag{9}$$

where

$$N_1 = (x_2 y_3 - x_3 y_2) + (y_2 - y_3)x + (x_3 - x_2)y,$$

$$N_2 = (x_3 y_1 - x_1 y_3) + (y_3 - y_1)x + (x_1 - x_3)y,$$

$$N_3 = (x_1 y_2 - x_2 y_1) + (y_1 - y_2)x + (x_2 - x_1)y$$

Substituting the element coordinates and displacement interpolations into the governing finite element equation derived from Eq. (9) yields

$$\left(\boldsymbol{K}_L + \boldsymbol{K}_{NL}\right)\Delta\boldsymbol{U} = \boldsymbol{R} - \boldsymbol{F} \tag{10}$$

where $\boldsymbol{K}_L$ and $\boldsymbol{K}_{NL}$ are, respectively, the linear and nonlinear stiffness matrices, $\boldsymbol{R}$ refers to the vectors of external applied nodal points loads, and $\boldsymbol{F}$ is the vector of node point force equivalent to the element stress.

To obtain accurate and consistent results, the structural problem is integrated into an updated Lagrangian formulation, and the resulting general nonlinear structural equation system is solved using the Newtion-Raphon method.

4. Strategy for fluid-structure coupling

Coupled fluid and structure interaction has attracted interests of many researchers, as reviewed by Lian et al.[12,13]. There are three major classes for fluid-structure coupling: fully coupled, closely coupled, and loosely coupled analyses. In this work, closely coupled analysis is utilized.

In the closely coupled analysis, the information exchanged is surface loads and displacement field: the former is mapped from CFD grid onto the airship structure grid, and the latter, from the airship structure grid onto CFD grid. As different meshes are used in fluid and structure computation, a technique is needed which links these individual modules. The thin plate spline interpolation is selected in this work to map the external load and the shape deformation onto structure and fluid solvers, respectively. To ensure the accuracy of the results, iterations are performed between the fluid and structural solvers. A coupled fluid-structure analysis diagram of the program is shown in Fig.1.

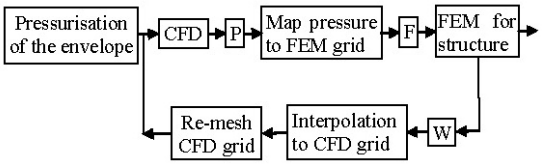

Fig.1 Coupled fluid-structure flow diagram

The transfer of surface displacement back to the CFD module implies the deformation of CFD boundary mesh. The transfinite interpolation[14], which has been typically used for regenerating meshes, is introduced to re-mesh the entire CFD domain for further computation.

5. Numerical results and discussion

5.1 *Pressure loaded-pretensioned square membrane*

A test problem is conducted to assess the performance of this work. The historical works of Han et al. [15] and Irvine [16] presented their studies of the deflection response of a pressure loaded-pretensioned square membrane, numerically and analytically, respectively. In Table 1, the results from our program is compared with the analytical solutions by Irvine and numerical results by Han et al. based on a square membrane with the following parameters: side length $a = 1520\text{mm}$, thickness $t = 1.46\times10^{-2}\,\text{mm}$, Young's modulus $E = 103\,\text{GPa}$, pressure $p = 241\text{Pa}$, tension per unit length $T = 1.75\text{N/mm}$. In our program, the membrane is discretized with 800 elements as shown in Fig.2. It is apparent that there exists good agreement between their results and ours.

Table 1 Comparison of deflection response of the square membrane

Deflection (mm)	Points on membrane					
	1	2	3	4	5	6
Irvine[16]	3.41	6.69	7.57	14.31	16.08	19.22
Han and Olson[15]	3.59	6.79	7.50	14.49	16.62	19.32
Present result	3.34	6.35	7.11	13.52	15.49	18.31

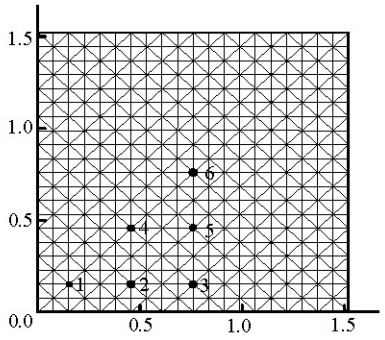

Fig.2 Discretization scheme for square membrane

5.2 Airship aerodynamics

To clarify the influence of the elastic deformation under aerodynamic force, we calculate the airships with different lengths and attack angles through the coupled fluid-structure computation. Two structural models are compared: the rigid model whose geometry has no deformation at all and the aeroelastic model whose geometry is deformed by aerodynamic load.

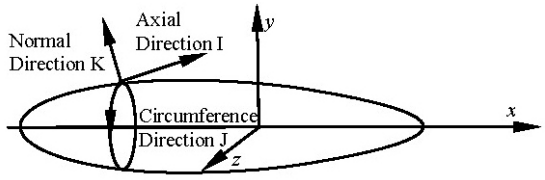

Fig.3 The directions of grid collocation on the airship

The axis of the airship is set to be *x*-direction (Fig.3). The total length *l* of the airship is 20 m, 60 m, 120m and 220m, respectively. The thickness ratio (d/l) of the airship body of revolution is 0.25. The vector of inflow velocity lies in the plane of $x-z$ and the attack angle is the inclination of the velocity vector and *x* axis. Both the incident flow and the airship are symmetric against the $x-z$ plane. Thus, in the calculation, only half of the airship is considered and the computation field turns to be half of the geometric field. To analyze the flow field, a structure grid is built in the hemisphere. The grid has 111 points in the axial direction, 73 points along the circumference direction and 63 points in the normal direction. For the FEM analysis, the unstructured grid employs 8162 nodes and 16320 triangular membrane elements on the airship.

The solution to fluid-structure interaction starts with the parameter from the trimmed rigid model. Then the simulation work is the pressurization of the airship envelope. After that the iterative solving between CFD and CSD is realized. The convergence criterion is based on the deformation of the airship structure. In general the approximately 10 iteration steps are necessary to obtain the results.

The drag coefficient C_D and the lift coefficient C_L are calculated based on the attack angle and the coefficient of axial force C_X, and the normal force C_Y. They can be written as

$$C_D = C_X \cos\alpha + C_Y \sin\alpha \tag{11}$$

$$C_L = -C_X \sin\alpha + C_Y \cos\alpha \tag{12}$$

The formulations for C_X and C_Y are

$$C_X = \frac{F_X}{1/2\,\rho U^2 S},\quad C_Y = \frac{F_Y}{1/2\,\rho U^2 S} \tag{13}$$

where F_x and F_y are, respectively, the axis and normal forces of aerodynamics, $S = V^{2/3}$ refers to the surface of the airship, and V is the volume of the airship.

The following empirical formulation for C_D is given by Khoury and Gillette[3] as a function of thickness ratio (d/l) of streamline bodies:

$$C_D = [0.172(l/d)^{1/3} + 0.252(d/l)^{1.2} + 1.032(d/l)^{2.7}]/Re^{1/6} \tag{14}$$

This coefficient of drag C_D is calculated on zero angle of attack.

As is shown in Table 2, the computation results are fairly close to those from the formula (14). Since the drag coefficient is quite sensitive in aerodynamic computation, all these findings can well justify the validity of our program.

Table 2 Coefficient of drag C_D of airship (Rigid model, α=0)

C_D	Length of airships (m)			
	20m	60m	120m	220m
Formula (14)	0.02757	0.02304	0.02058	0.01854
Present result	0.02545	0.02139	0.01942	0.01778

Figures 4 and 5 reflect the difference of drag coefficient characteristics $C_D(\alpha)$ between the two models, while Figs.6 and 7 show the difference of lift coefficient C_L. As is shown in the figures, the aeroelastic model exhibits slightly larger value than the rigid one both for drag coefficient and lift coefficient. It is apparent that the difference of the drag coefficient between the two models increases with the rising of the lengths of airships, and so does the lift coefficient. This is owing to the fact that the flexibility of the airship increases with its size going up. The difference in the coefficient of drag C_D of the 220 m airship as the angle of attack is 5 is found to be greater than 2% and the lift coefficient generated in the aeroelastic model slightly exceeds 4%. This information is quite helpful to gain more insight into the stratosphere airship aerodynamics.

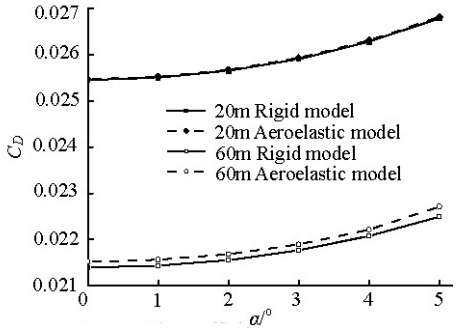

Fig.4 The drag coefficient C_D of the airship

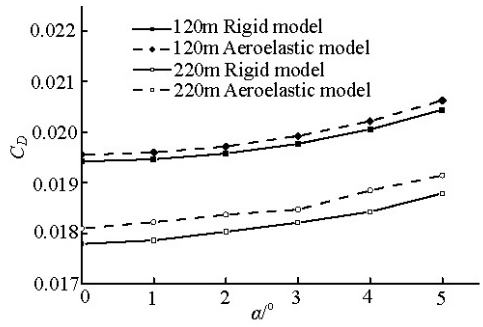

Fig.5 The drag coefficient C_D of the airship

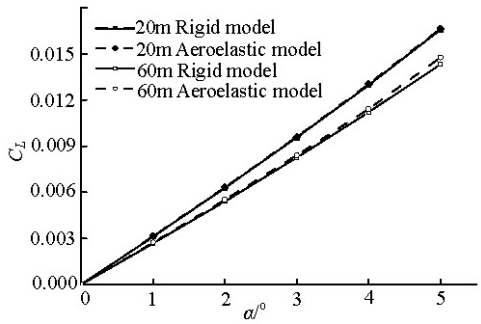

Fig.6 The lift coefficient C_L of the airship

The contours of pressure coefficient of 60 m long and 220 m long airships in different models are plotted in Figs.8-11. It seems that the low-pressure area extends a bit in the aeroelastic model. This is possibly due to the fact that when the flexibility of the airship is taken into account the deformation in the low-pressure area turns greater, resulting from the ascending of the difference of pressure inside and outside the airship. The larger the airship is, the more conspicuous the phenomenon. By contrasting the detailed fluid flows around the rigid and aeroelastic models, we can better evaluate the technologies of the stability and control of the airship.

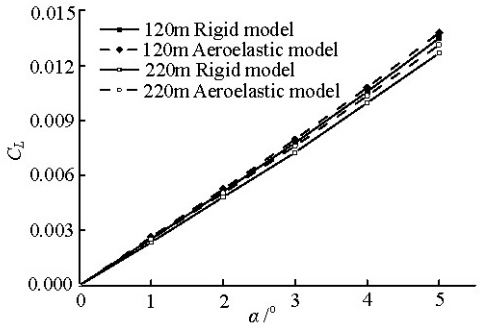

Fig.7 The lift coefficient C_L of the airship

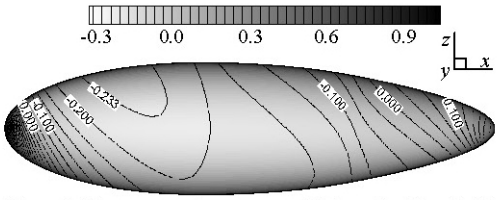

Fig.8 The contour of pressure coefficient C_P of the airship (60 m, rigid model, α=5°)

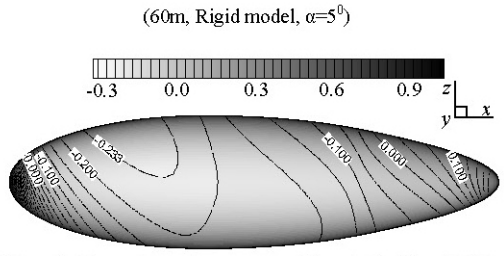

Fig.9 The contour of pressure coefficient C_P of the airship (60 m, aeroelastic model, α=5°)

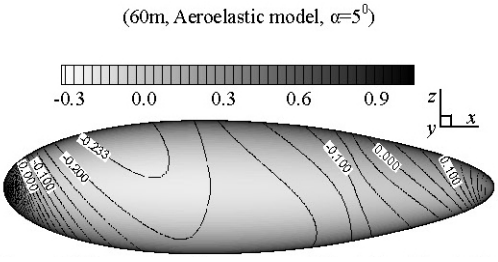

Fig.10 The contour of pressure coefficient C_P of the airship (220 m, rigid model, α=5°)

Figures 12 and 13 show the contour of deformation of the airship. It is clear that the deformation is comparatively great in the central body of large cross-section. The maximal deformation frequently appears around where the maximal cross-section lies.

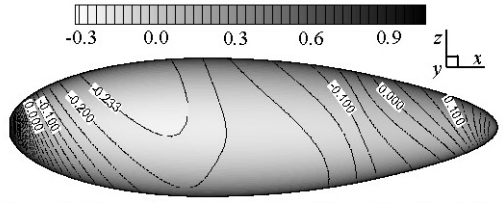

Fig.11 The contour of pressure coefficient C_P of the airship (220 m, aeroelastic model, α=5°)

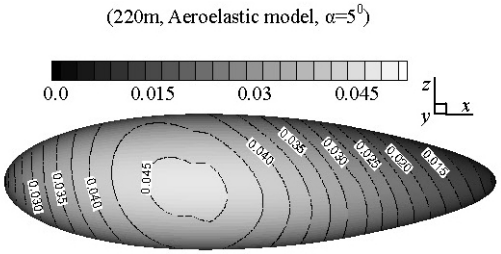

Fig.12 The contour of deformation of the airship (60 m, α=5°)

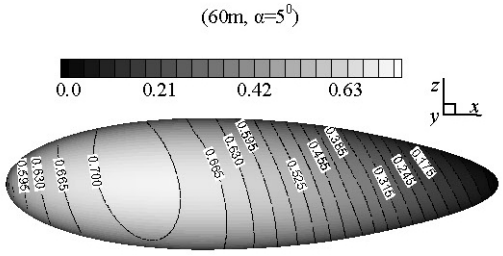

Fig.13 The contour of deformation of the airship (220 m, α=5°)

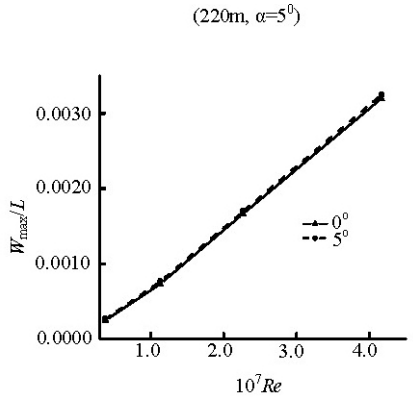

Fig.14 Maximal displacement of the airship versus *Re*

Figure 14 compares the ratio, $w_{\max}/l$, of the maximal deformation to the total length of the airship with the Reynolds number. With the rising of Reynolds number, the ratio increases.

6. Conclusions

A three-dimensional interactive analysis of airship aeroelasticity is presented. The flow, modeled as a viscid fluid, is solved using a finite volume method. To account for the deformation of the airship a three-dimensional membrane model is proposed. A nonlinear finite element method with triangular elements of spatial discretization is employed to solve the structure equations of airship. A coupled strategy between the two field equations solvers is developed. The performance of the FVM and FE programs is assessed by examining independent flows and structure problems. Good agreement is achieved in the compared quantities.

Based on this computational capability the study of the aeroelastic characters of airships is conducted. The effect of shape change of the aeroelastic model on the aerodynamic performance is detailed. The results show that aerodynamic coefficients--the drag coefficient and lift coefficient of the aeroelastic model are slightly higher than those of the rigid one. All the results will encourage the development of more detailed and more accurate aerodynamic and dynamic models of the airship culminating in extremely comprehensive nonlinear simulation models.

References

[1] BESSERT N., FREDERICH O. Nonlinear airship aeroelasticity [J]. **Journal of Fluids and Structures**, 2005, 21(8): 731-742.

[2] WANG Xiao-liang, SHAN Xue-xiong. Aerodynamic estimation for stratosphere airship [J]. **Chinese Quarterly of Mechanics**, 2006, 27(3): 295-304 (in Chinese).

[3] KHOURY G. A., GILLETT J. D. **Airship technology** [M]. Cambridge, UK: Cambridge University Press, 1999.

[4] WILCOX D. C. **Turbulence modeling for CFD** [M]. California: DCW Industries, Inc., 1996.

[5] LIEN F. S., LESCHZINER M. A. Computational modeling of 3D turbulent flow in S-diffusor and transition Ducts [C]. **2nd International Symposium Engineering Turbulence Modeling and Experiments.** Amsterdam, The Netherlands, 1993, 217-233.

[6] HUANG Zheng-yu, MIAO Guo-ping. A Matrix-free implicit method for incompressible flow around 3D complex underwater bodies [J]. **Journal of Hydrodynamics, Ser. B**, 2006, 18(2): 192-198.

[7] FERZIGER J. H., PERIC M. **Computational methods for fluid dynamics** [M]. Berlin, Germany: Springer-Verlag, 1996.

[8] LIU Xiao-dong, HUA Zu-lin. Numerical simulation for shallow flow and pollutant dispersion based on quad-tree messes [J]. **Journal of Hydrodynamics, Ser. B**, 2006, 18(2): 161-169.

[9] ODEN J. T., SATO T. Finite strains and displacements of elastic membranes by the element method [J]. **International Journal of Solids and Structures**, 1967, 3(4): 471-488.

[10] NEWMAN B. G. Aerodynamics theory for membrane and sails [J]. **Progress in Aerospace Sciences**, 1987, 24(1): 1-27.

[11] ZIENKIEWICZ O. C., TAYLOR R. L. **The finite element method: basic formulation and linear problems** [M]. New York: MacGraw-Hill, 1989.

[12] LIAN Y. S., SHYY W. and VIIERU D. et al. Membrane wing aerodynamics for micro air vehicles [J]. **Progress in Aerospace Sciences**, 2003, 39(6): 425-465.

[13] SMITH M. J., HODGES D. H. and CESNIK C. E. S. Evaluation of computational algorithms for fluid-structure interface [J]. **Journal of Aircraft**, 2000, 37: 282-294.

[14] ERIKSSON L. E. Generation of boundary-confirming grids around wing-body configurations using transfinite interpolation [J]. **AIAA Journal**, 1982, 20(10): 1313-1320.

[15] HAN P. S., OLSON M. D. Interactive analysis of wind-loaded pneumatic membrane structures [J]. **Computers and Structures**, 1987, 25(5): 699-712.

[16] IRVINE H. M. Analytical solution for pretensioned cable nets [J]. **The Engineering Mechanics Division**, **ASCE,** 1976, 102(1): 43-57.